



ELSEVIER

Available online at www.sciencedirect.com

SCIENCE @ DIRECT®

Nuclear Instruments and Methods in Physics Research B 204 (2003) 570–581

NIM B
Beam Interactions
with Materials & Atomswww.elsevier.com/locate/nimb

Slow RI-beams from projectile fragment separators

Michiharu Wada ^{a,*}, Yoshihisa Ishida ^a, Takashi Nakamura ^a,
Yasunori Yamazaki ^a, Tadashi Kambara ^a, Hitoshi Ohyama ^a, Yasushi Kanai ^a,
Takao M. Kojima ^a, Youichi Nakai ^a, Nagayasu Ohshima ^a, Atsushi Yoshida ^a,
Toshiyuki Kubo ^a, Yukari Matsuo ^a, Yoshimitsu Fukuyama ^a, Kunihiro Okada ^b,
Tetsu Sonoda ^c, Shunsuke Ohtani ^d, Koji Noda ^e, Hirokane Kawakami ^f,
Ichiro Katayama ^f

^a Atomic Physics Laboratory, RIKEN, 2-1 Hirosawa, Wako, Saitama 351-0198, Japan

^b Department of Physics, Sophia University, 7-1 Kioicho, Chiyoda, Tokyo 102-8554, Japan

^c Cyclotron and Radioisotope Center, Tohoku University, Sendai 980, Japan

^d Institute of Laser Science, University of Electro-Communications, Chofu 182-8585, Japan

^e National Institute for Radiological Science, Chiba 263-8555, Japan

^f Institute of Particle and Nuclear Studies (IPNS), KEK, Tsukuba 305-0801, Japan

Abstract

The projectile fragment separator provides a wide variety of short-lived RI-ions with less restrictions on their chemical property or lifetime limit. The beam energy and quality is, however, not adequate for low-energy beam experiments, in particular for trapping experiments.

Recently, one has proposed to obtain a low-energy beam from an energetic RI-beam leaving a projectile fragment separator by using a large gas-catcher and an rf ion-guide system. In off-line and in on-line test experiments, the principle of the rf ion-guide was proven. An overall efficiency of 0.2% for 70 MeV/u ⁸Li from the RIKEN projectile fragment separator (RIPS) was obtained so far.

© 2003 Elsevier Science B.V. All rights reserved.

PACS: 29.25.Rm; 41.85.Ar

Keywords: RI beam; Gas catcher; Rf ion-guide; ⁸Li; Projectile fragment separator

1. Introduction

In the past, low-energy RI-beams have been provided mainly by so-called ISOL (isotope separator on-line) facilities while high-energy RI-beams have been obtained at projectile fragment separator facilities. In the next generation of RI-beam facilities both try to intrude into the other territories by utilizing additional devices. The ISOL facilities add post-accelerators to obtain high-energy RI-beams which have the same high quality as stable nuclear ion beam accelerators except for intensity. The fragment separator

rator on-line) facilities while high-energy RI-beams have been obtained at projectile fragment separator facilities. In the next generation of RI-beam facilities both try to intrude into the other territories by utilizing additional devices. The ISOL facilities add post-accelerators to obtain high-energy RI-beams which have the same high quality as stable nuclear ion beam accelerators except for intensity. The fragment separator

* Corresponding author. Tel.: +81-48-467-9487; fax: +81-48-462-4644.

E-mail address: mw@riken.go.jp (M. Wada).

facilities, on the other hand, add deceleration and cooling devices to obtain low-energy RI-beams which are less limited by chemical properties nor lifetimes of the nuclides. Fig. 1 shows a typical yield-map of an ISOL facility and that of a fragment separator facility which indicates that there are many missing regions of available nuclides in the conventional ISOL facility while the fragment separator facility covers a wide area of the nuclear charts.

At RIKEN a radioactive beam factory (RIBF) is under construction. The new facility consists of several stages of heavy-ion cyclotrons that will provide 1-pμA, 350 MeV/u heavy-ion beams, two large projectile fragment separators (Big RIPS) and several storage rings (MUSES) [1,2]. The projectile fragment separator provides a wide variety of radioactive nuclear ions. The beam energy and quality, however, is not adequate for low-energy beam experiments, in particular for trapping experiments in Penning traps or in similar devices that allow a variety of high-precision experiments.

We have proposed and tested a new scheme to collect such energetic RI-beams by using an extended gas cell of an IGISOL type (ion-guide isotope separator on-line) [3–5] and a superimposed dc and rf electric guiding field in the cell (rf ion-guide) [6–9]. In this paper we discuss stopping energetic RI-beams in a catcher gas cell and ma-

nipulation of the ion motion in the gas cell. Recent on-line experiments at the RIKEN accelerator facility are also reported.

2. Stopping ions in a gas cell and extraction

The RI-beams from a projectile fragment separator typically have an energy of 100 MeV/u and an energy spread of a few percent. To decrease the absolute energy, an energy degrader must be placed upstream of the catcher gas cell. However, the energy spread becomes very large in such a device due to multiple collisions in the degrader. After passing through a 25.1 mm thick Al degrader a mono-energetic ^{11}Be beam of 100 MeV/u causes an energy distribution that spreads from 0 to 9 MeV/u according to numerical calculations. In the case of ^{78}Ni of 100 MeV/u and a 3.8 mm thick degrader the distribution ranges from 0 to 3 MeV/u. This situation becomes worse for actual RI-beams from a fragment separator, so that we must employ a wedge shaped degrader in combination with the momentum dispersive ion optics of the separator to reduce the energy spread at the position of the gas cell as much as possible.

The stopping capability of He gas is also mass dependent. For a typical 2 m long gas cell with 0.2 bar He gas, the stopping capability is 2 MeV/u for

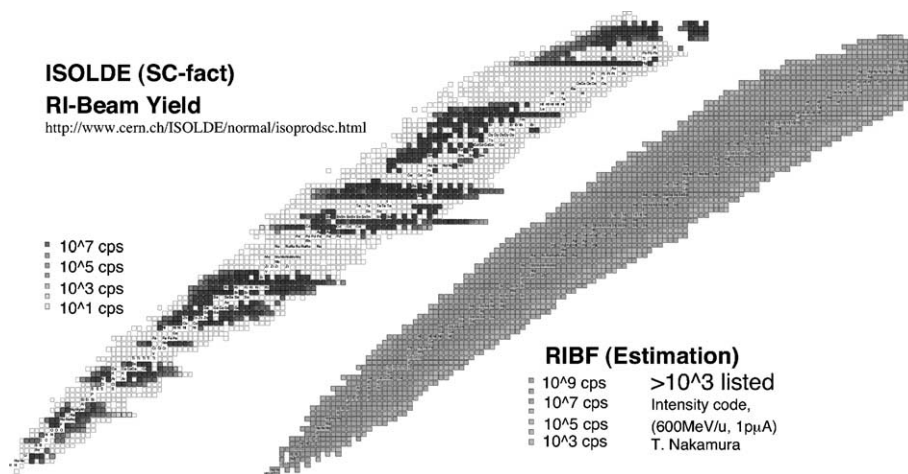


Fig. 1. RI-beam yield plotted on a nuclear chart. (a) Typical yield at ISOLDE CERN (left). (b) Estimated yield from BigRIPS at RIKEN RIBF, an RI-beam factory (right).

light nuclides such as Li, but 5 MeV/u for nuclides heavier than $A = 40$.

In a conventional IGISOL system a gas cell was typically a few cm thick. Reaction products recoiling out from the target were stopped in He gas, some as neutrals but a large fraction as singly charged ions due to the high ionization potential of He. The stopped ions are then transported to the exit nozzle of the cell by the gas flow. Since the cell is small, the extraction time typically in less than 100 ms, fast enough for reasonably short-lived nuclei. But the stopping capability of such a small cell is only in the order of 10 keV/u which is too small for a high-energy beam of a fragment separator. A simple enlargement of the gas cell would delay the extraction of ions by many minutes. This would cause severe losses of ions not only due to the limited lifetimes but also due to losses caused by charge exchange of the ion with residual impurities and diffusion to the walls of the cell.

Since an ion has a charge, use of an electric field to accelerate the extraction would be useful. However, a *simple* static field does not work properly. Since the ion motion in a gas of such

high pressure is very different from that in vacuum. In a gas the ion follows the line of the electric force directly and its velocity is proportional to the electric field. If one placed a simple anode–cathode mesh electrode pair in a gas cell, ions move toward the cathode electrode. However, they are collected on the surface of the cathode mesh where the lines of the electric force terminate.

There are two major different methods, so far proposed or tested, to overcome this problem:

- (1) use of a gas flow at the cathode electrode,
- (2) use of an rf-barrier field at the cathode electrode.

The first method is relatively simple to build and can be operated at higher pressures if the gas flow is fast enough to overcome the electric force at the nozzle. In the second method, the ion motion is controlled by an electric field, so that gas flow is not required anymore. A fine electrode structure allows to make the exit nozzle size small which reduces the gas load in the downstream instruments. However, the barrier force due to a gradient of the rf-field is inversely proportional to

Table 1
Large gas cell developmental activities to collect energetic RI-beams

RI-beam energy Isotope separator	Laboratory	Gas pressure Cell size	Guiding force	Status/Comment
<i>High energy</i>				
~100 (350) MeV/u PF (RIPS)	RIKEN/Japan	~130 mbar 40 cm \varnothing \times 200 cm	DC + RF funnel, DC + RF carpet	On-line test with 70 MeV/u ^8Li
100–1000 MeV/u PF (FRS)	GSI/Darmstadt	0.5–1 bar 20 cm \varnothing \times 125 cm	DC + RF funnel	Under construction
~100 MeV/u PF (A1900)	NSCL/MSU	<5 bar 5 cm \varnothing \times 50 cm	DC + Gas flow	Under construction
<i>Medium energy</i>				
~5 MeV/u GARIS, RS	ANL/Argonne	~150 mbar 10 cm \varnothing \times 20 cm	DC + RF-funnel + Gas flow	On-line test Cs etc., mass measurements ^{68}Ge , ^{68}As , etc.
~5 MeV/u VF (SHIP)	GSI/Darmstadt	~0.1 bar 17 cm \varnothing \times 18 cm	DC + RF-funnel + Gas flow	On-line test with stable Ca
5–40 MeV/u PF, GARIS	KVI/Groningen		DC + RF or Gas flow	Design phase
~1 MeV/u n-fission + IGISOL	CYRIC/Sendai	~100 mbar 24 cm \varnothing \times 30 cm	DC + Gas flow	Start on-line test

The abbreviations are PF: projectile fragment separator, GARIS: gas filled recoil isotope separator, VF: velocity filter, IGISOL: ion-guide isotope separator on-line.

the square of the gas pressure, as will be discussed later, so that the maximum possible pressure is limited.

There are several attempts to employ such a large gas cell to collect energetic RI-beams (see Table 1). We have proposed to use the latter method and named it the *rf ion-guide*.

3. Principle of the rf ion-guide

An overview of the entire system is shown in Fig. 2. The energetic RI-beams coming from the fragment separator are passed through a degrader. The medium energy beam, thus obtained, is then injected into a large He gas cell to thermalize the ions. The stopped ions must be extracted quickly to the vacuum and transferred to the downstream instruments in an ultra-high vacuum. A static electric field is applied between the cell as an anode and the exit as a cathode. In the rf ion-guide, the cathode electrode is replaced by a series of ring electrodes to which rf voltages are applied in addition to dc potentials with the idea that the average force due to the rf gradient field drives the ions away from the electrodes (Fig. 3). The fun-

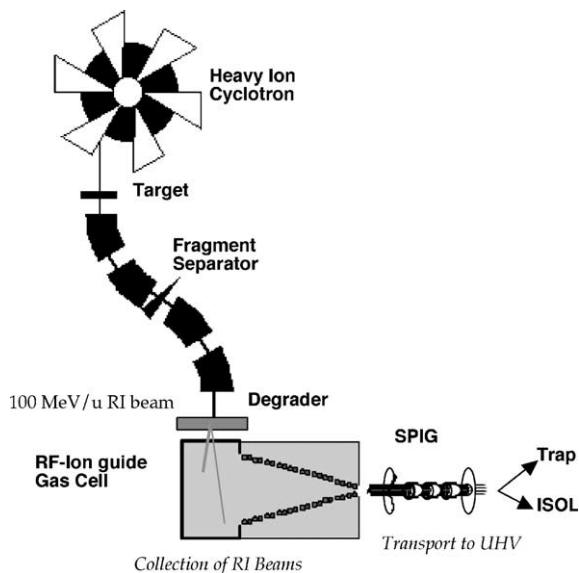


Fig. 2. Schematic diagram of an rf ion-guide system placed downstream of the fragment separator at a RI-beam facility.

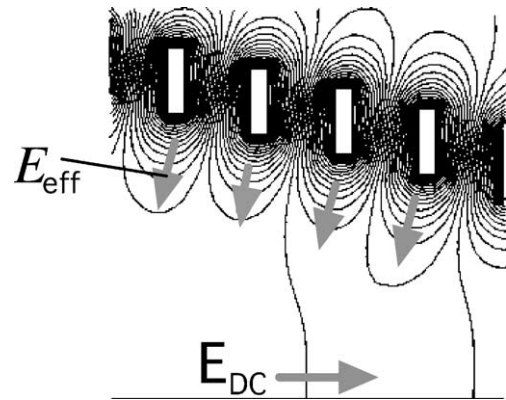


Fig. 3. Rf gradient field produced by a series of ring electrodes rotationally symmetric to the shown lower line. The electrodes also provide a superimposed dc-field E_{DC} . Note that the ions experience an effective electric field E_{eff} , driving them away from the rf-electrodes.

damental principle is the same that is used in an rf quadrupole ion trap introduced by W. Paul in 1953. The first experimental test of a funnel structure for manipulating charged micro-particles in 1 bar of air was performed by a Tokyo group in early 1970s [12]. They called this an *rf-hopper* or an *electric field curtain*. This rf funnel structure has also been used for collecting ions in an electro-spray ion-source for mass spectroscopy [13]. We incorporated this rf *funnel* structure into the ion-guide gas cell to manipulate singly-charged ions of short-lived nuclei.

The extracted ions are transported by SPIG [10] through a number of differential pumping sections toward experimental instruments in an ultra-high vacuum. The transport line also has bunching capabilities [11].

3.1. Simulation

In order to understand the operation of the rf ion-guide, we performed several analyses of the ion motion. The fundamental equation of motion is

$$m\ddot{\mathbf{r}} = e\mathbf{E}(r, t), \quad (1)$$

where m is the mass of the ion and \mathbf{E} the electric field. A microscopic Monte Carlo simulation can start from this equation directly. The presence of a

buffer gas is taken into account by including classical potential scattering at each collision between the ion and gas atoms or molecules. The scattering angle in the center of mass system is

$$\theta_{\text{CM}}(b, E) = \pi - 2 \int_{R_{\text{min}}}^{\infty} \frac{b}{r^2} \frac{dr}{\sqrt{1 - (b/r)^2 - V(r)/E}}, \quad (2)$$

where b is the impact parameter, E the relative energy and R_{min} is obtained from $1 - (b/R_{\text{min}})^2 - V(R_{\text{min}})/E = 0$. We have chosen a scattering potential

$$V(r) = \frac{\epsilon}{2} \left[(1 + \gamma) \left(\frac{r_m}{r} \right)^{12} - 4\gamma \left(\frac{r_m}{r} \right)^6 - 3(1 - \gamma) \left(\frac{r_m}{r} \right)^4 \right], \quad (3)$$

with the parameters γ , ϵ and r_m being taken from [14].

The dc and rf electric field maps were calculated by POISSON [15], obtaining the total electric field as function of time:

$$\mathbf{E}(r, t) = \mathbf{E}_{\text{dc}}(r) + \mathbf{E}_{\text{rf}}(r) \cos(\Omega t). \quad (4)$$

Typical ion trajectories are shown in Fig. 4 illustrating the part of the cell that is close to the exit. The electrode structure consists of a nozzle and a large funnel. The nozzle is built from 70 ring electrodes with intervals of 0.3 mm. It has apertures of 0.4 mm at the exit and 11.2 mm at the top. In the large funnel the interval of each electrode is 0.5 mm and the aperture at its bottom is 10 mm.

The microscopic simulation clearly shows the transport of ions in the rf ion guide. However, an analytical approach is helpful to understand the various physical processes. We employed the *mobility* (μ) of ions in the gas to simulate the effect of multiple collisions as a frictional force. The equation of motion is

$$m\ddot{\mathbf{r}} + \frac{e}{\mu}\dot{\mathbf{r}} = e\mathbf{E}(r, t). \quad (5)$$

If we define the velocity relaxation time as $\tau_v = m\mu/e$, Eq. (5) becomes

$$\ddot{\mathbf{r}} + \frac{1}{\tau_v}\dot{\mathbf{r}} = \frac{e}{m}(\mathbf{E}_{\text{dc}}(r) + \mathbf{E}_{\text{rf}}(r) \cos(\Omega t)). \quad (6)$$

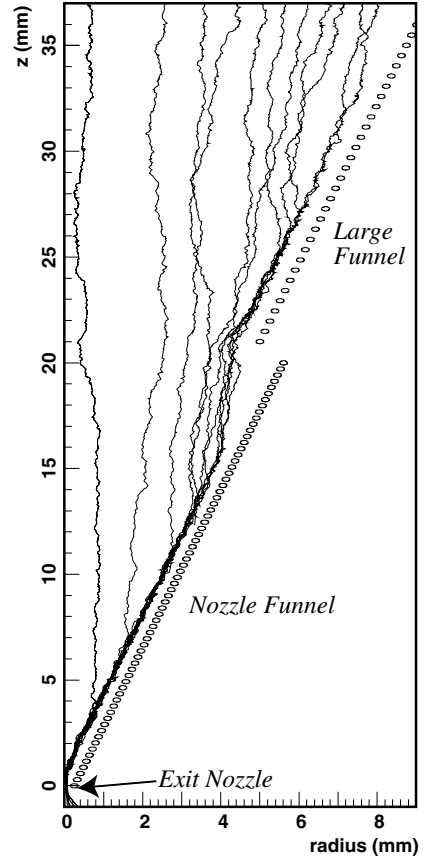


Fig. 4. Typical ion trajectories in a double rf-funnel structure as determined by microscopic particle simulation for ^8Li ions in 30 Torr He gas. The rf voltage between neighboring electrode rings is 80 V at 10 MHz. The superimposed dc field is 12 V/cm.

This permits two different ways of analysis. Assuming that the field close to the electrodes is a quadrupole field, Eq. (6) simplifies to Mathieu's equation,

$$u'' + 2pu' + (a - 2q \cos 2\tau)u = g, \quad (7)$$

with the dimension-free parameters $a = 8eV_{\text{dc}}/m r_0^2 \Omega^2$ characterizing the dc offset and $q = 4eV_{\text{rf}}/m r_0^2 \Omega^2$ the rf field strength. Here $p = e/m\mu\Omega = 1/\tau_v\Omega$ characterizes the gas pressure, $g = 4eE_{\text{dc}}/m\Omega^2$ the external force while $\tau = \Omega t/2$. The terminal voltages of the quadrupole electrodes are V_{rf} and V_{dc} and the half distance of the electrode is r_0 . The stability analysis of an ordinary Mathieu equation can be performed from Eq. (6) [16].

Another way to analyze Eq. (6) is the pseudo-potential approach. The rf electric field is averaged over a cycle to deduce the strength of the effective electric field due to the rf gradient field. We omit the static field in Eq. (6) and split the motion of an ion into a slow average motion \bar{r} and a small oscillation motion $\rho(t)$ as

$$r = \bar{r} + \rho(t) = \bar{r} + c\mathbf{E}_{\text{rf}}(r) \cos(\Omega t + \beta). \quad (8)$$

The coefficient c here is deduced by inserting \dot{r} and \ddot{r} as determined from Eq. (8) into Eq. (6). Then the small oscillation is described by

$$\rho(t) = -\frac{e}{m\Omega} \frac{\mathbf{E}_{\text{rf}}(r)}{\sqrt{\Omega^2 + 1/\tau_v^2}} \cos(\Omega t + \beta), \quad (9)$$

$$\tan \beta = \frac{1}{\tau_v^2 \Omega^2}.$$

The average force \bar{F} due to the gradient rf field is

$$\begin{aligned} \bar{F}(\bar{r}) &= e \langle \mathbf{E}_{\text{rf}}(\bar{r}) \cos \Omega t + [\nabla|_{r=\bar{r}} \mathbf{E}_{\text{rf}}(r)] \rho(t) \cos \Omega t \rangle_{\text{av}} \\ &= -\nabla \mathbf{E}_{\text{rf}}^2(\bar{r}) \frac{e^2}{4m} \frac{1}{(\Omega^2 + 1/\tau_v^2)}. \end{aligned} \quad (10)$$

Eq. (10) is simplified in two extreme cases, the vacuum limit and the high pressure limit, respectively,

$$\bar{F}(\bar{r}) = \begin{cases} -\nabla \mathbf{E}_{\text{rf}}^2(\bar{r}) \frac{e^2}{4m\Omega^2} & \text{for } \Omega^2 \tau_v^2 \gg 1 \text{ (vacuum),} \\ -\nabla \mathbf{E}_{\text{rf}}^2(\bar{r}) \frac{e^2}{4m\tau_v^2} & \text{for } \Omega^2 \tau_v^2 \ll 1 \text{ (high pressure).} \end{cases} \quad (11)$$

If we assume again a quadrupole field close to the electrode, the average force in the high pressure limit is

$$\bar{F}_{\text{hp}} = -\frac{e^2}{4m} \tau_v^2 \frac{8V_{\text{rf}}^2}{r_0^3} \left(\frac{r}{r_0} \right) = -m\mu^2 \frac{V_{\text{rf}}^2}{r_0^3} \left(\frac{r}{r_0} \right). \quad (12)$$

Assuming the mobility being simply proportional to the reciprocal of the gas pressure, ions are manipulated by weaker rf field in lower gas pressure. This is even more so for heavier ions. In total, heavier ions are extracted quicker than lighter ions. It should be noted, however, that the pseudo-potential analysis does not provide information about the stability of the ion motion.

4. Experiment at KEK-Tanashi and RIKEN

4.1. Off-line test with Ta^+ ions

The first test gas cell was build in 1998 and tested at KEK-Tanashi. In a 30 cm long gas cell, 80 electrodes at intervals of 2.5 mm were arranged to form a funnel structure with an rf voltage and different dc offsets being applied to each electrode. Fig. 5 shows a schematic diagram of this gas cell. Ta^+ ions were formed in the small cell shown in Fig. 5 by a pulsed YAG laser irradiation. The ions are, then, injected into the rf ion-guide cell by a gas flow. The source current was monitored throughout the measurement for normalization. A typical current of 100 pA was obtained at an irradiation frequency of 10 Hz and a gas flow rate of 3 Torr l/s. The transported ions were detected by a Faraday cup located downstream of the ring electrodes.

A typical experimental result is shown in Fig. 6. The effect of the rf electric field can be seen. At 20 Torr He gas pressure and an rf voltage of 150 V_{pp} a transmission of $\sim 70\%$ was obtained. The voltage was limited by a discharge that occurred around the feedthroughs. The transmission decreased when the gas pressure was increased. For higher pressures, higher rf voltages are required. It should be noted that the Faraday cup measurement cannot distinguish whether the ions are Ta^+ or impurity ions.

The gas pressure of 20 Torr used in the test experiment is too low for realistic applications. In order to stop a radioactive beam of 5 MeV/u in a

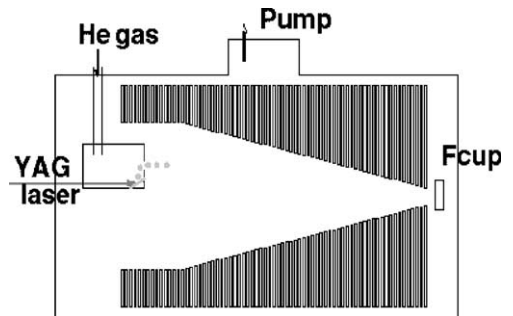


Fig. 5. Off-line test setup for the transport of Ta^+ ions. A stack of metal plates was used to form rf ring-electrodes (left). The gap between each plate was 2.5 mm.

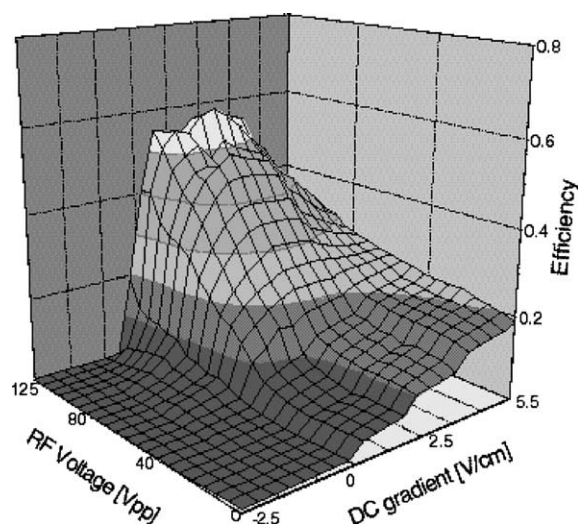


Fig. 6. Transmission efficiency as function of the rf-amplitude and the dc field applied to the ring electrodes of Fig. 5.

gas cell, a pressure of 150 Torr and a thickness of 2 m seems necessary.

According to Eq. (12), an effective way to increase the operating pressure is to decrease r_0 , which corresponds to a reduction of the interval of the electrodes. For an electrode structure with an interval of 0.5 mm, a similar transmittance would be achieved in a high pressure He gas of 150 Torr.

4.2. On-line test of the POP system

After the off-line test, we constructed a proof-of-principle (POP) system for on-line test experiments. The on-line tests were performed at the RIKEN projectile fragment separator RIPS [17] that provides a 70-MeV/u ^8Li ion beam with an intensity of $\sim 10^6$ atoms/s from a primary beam of 70-MeV/u ^{13}C and a production target of ^9Be . We chose ^8Li for the test ion beam, since the detection of ^8Li , which emits two alpha particles after the β -decay, is efficient and reliable. Although lighter ions are harder to manipulate in the gas cell and stopping efficiency is poorer, we tested with ^8Li ions.

The fragment separator consists of two dipole magnet and an energy degrader between the two magnets. The first magnet selects the fragment ions according to A/Z and the second magnet accord-

ing to $\sim A^{2.5}/Z^{1.5}$, since the dependence of energy loss in the degrader is different for Z and A . The separator thus provides pure isotopic ions in many cases. Although there are many impurity ions, we used only half of the separator. An advantage of using only one half is that we can put our system at the momentum dispersive focal point. It allows to employ a wedge shaped energy degrader for mono-energetic deceleration (Fig. 7). The impurity ions, on the other hand, can be eliminated by the so-called range separation: heavier ions such as $^{10,11}\text{Be}$ stop in the degrader and lighter ions such as ^3H just pass through the gas cell.

A schematic diagram of the POP setup is shown in Fig. 9(a). The gas cell is a simple vacuum vessel with a diameter of 10 cm and a length of 70 cm. This rf-funnel is a double funnel structure. The larger one has an entrance aperture of 10 cm diameter and an exit aperture of 1 cm. The smaller one has an entrance aperture of 12 mm diameter and an exit aperture of 0.5 mm (Fig. 8). Both are build of flexible printed circuit boards. The interval between each ring electrode pattern is 0.5 mm for the large one and 0.3 mm for the small one. The two funnel structures are stacked to transport ions from the entire cell to the exit.

The stopped ^8Li ions in the cell are pulled by static electric fields into the funnel where the rf

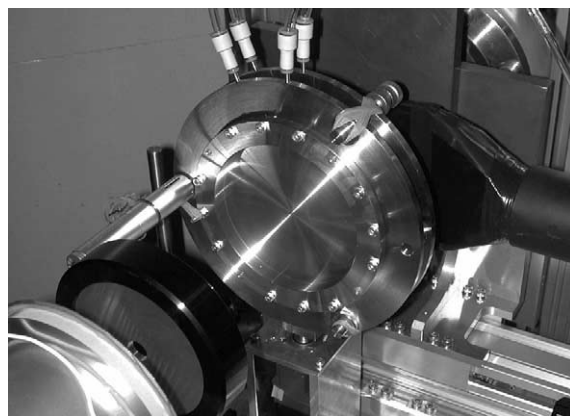


Fig. 7. Beam diagnostics devices as well as the wedge shaped energy degrader placed at the second momentum dispersive focal position downstream of the first dipole magnet of RIPS at RIKEN RARE. The degrader can be adjusted in thickness and wedge angle to provide a mono-energetic beam at the gas cell.

barrier-field protects the ions from collisions with the electrodes. We extracted the ions orthogonal to the incoming ^8Li beam in order to avoid the direct implantation of primary ions into the detector and also to make certain that the ions are transported

by the electric field, not only from the region very close to the exit.

The transported ^8Li ions were collected on a silicon detector and delayed- α decay was observed for their detection. The overall efficiency, defined as number of observed α -decay divided by total ^8Li ions from RIPS, of the POP system was $\sim 10^{-4}$ as shown in Fig. 9(b). Since so far no mass analyses were performed for the extracted ions, the detected ^8Li ions were not confirmed as singly-charged atomic ions. However, we assumed that most of the detected ^8Li were not molecular ions because molecular ions generally have smaller mobility in a gas so that they were hard to be manipulated in the present rf gradient field. A mass analyzer which will be connected behind the gas cell is under preparation. We compared the yield at gas pressures of 30 and 60 Torr. The yield at 60 Torr was lower than at 30 Torr, since probably the rf amplitude was too low for transporting ^8Li ions in He gas of 60 Torr. We also tested dependence of the yield on the length of the cell. The longer cell showed a higher yield than a shorter one. This indicates that even if ions are stopped in the region very far from the exit they were transported by the electric field.

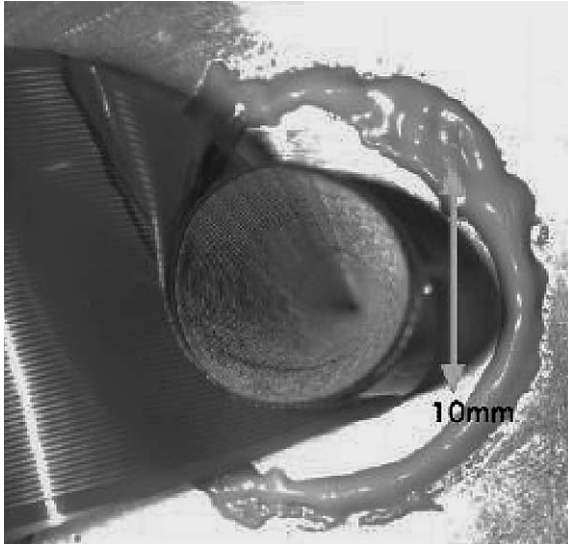


Fig. 8. Nozzle of the rf-funnel structure made of a flexible printed circuit board.

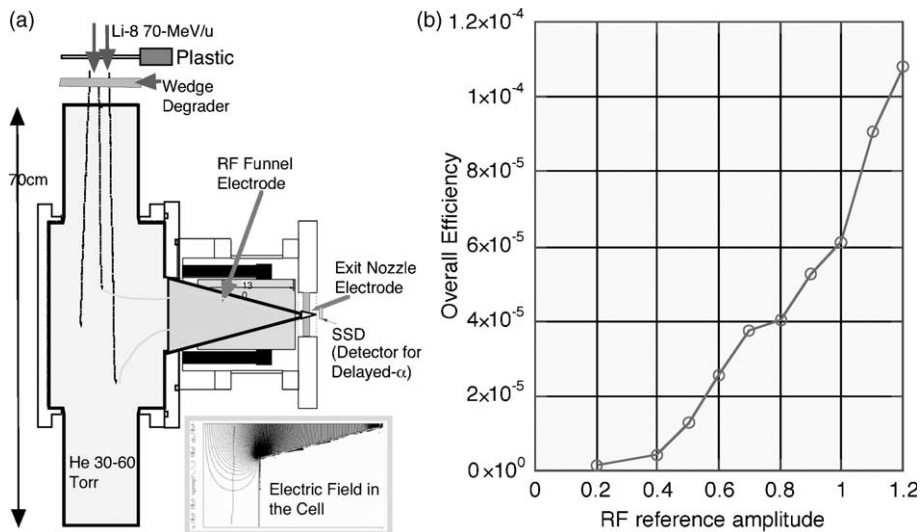


Fig. 9. (a) Experimental setup of the POP system. (b) Overall efficiency plotted as function of applied rf voltage. The gas pressure in the gas cell was 30 Torr, the dc field 10 V/cm, the maximum rf amplitude 50 V at 10 MHz.

The radial acceptance of the cell for the extended beam after the degrader was measured to be 30% using a collimated beam. The stopping capability of the 30 Torr gas cell was 0.43% as deduced from a range calculation, the measured energy distribution after the energy degrader, and the radial acceptance of the cell. Thus the overall efficiency can be separated into the gas stopping efficiency of 0.43% and the ion-guide efficiency of 2.4%. The first is limited by the geometry of the cell and the pressure of the He gas. The second by the present rf voltage limitation of 50 V.

4.3. On-line test of the 2 m gas cell

Based on the experience with the POP system a new system was constructed. The new gas cell is 40 cm in diameter and 2 m in length (Fig. 10). It is capable of in-line extraction as well as orthogonal extraction. In the POP system, rf divider circuits were placed outside of the cell and many long cables transported the power through feedthroughs resulting in large capacities and high heat dissipation. The new rf electrodes consist of two layers of planar printed circuit boards (PCB). The top one has a diameter of 29 cm with 280 ring electrode and a central hole of 10 mm. The bottom one has a diameter of 3 cm with 48 rings and an exit nozzle of 0.6 mm (see Fig. 11). We named this

structure the *rf-carpet*. A numerical simulation for typical ion trajectories in the rf carpet are also shown in Fig. 12. The rf divider circuits are soldered to the back surface of the PCB and the matching coil and feedthroughs have water cooling capabilities. Typical operating parameters are now 15 MHz and 150 V.

The field parameter dependence to the overall efficiency at 100 Torr He was measured as shown in Fig. 13. Since the rf carpet consists of two independent layers, the dependence was measured

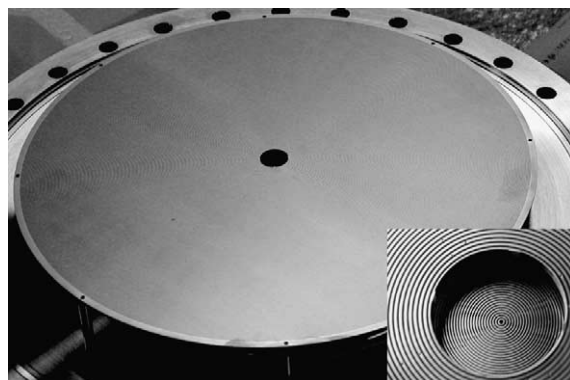


Fig. 11. The rf-carpet electrode made of two layers of planar printed circuit boards. The upper board is a disk of 29 cm diameter with 280 ring electrodes and a central hole of 10 mm. The bottom board is a disk of 3 cm diameter with 43 ring electrodes and an exit nozzle of 0.6 mm.

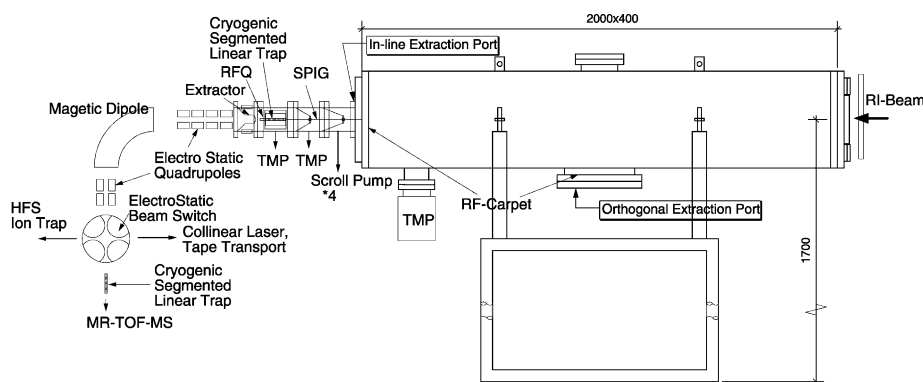


Fig. 10. The 2 m long gas cell of 0.4 m diameter placed downstream of the RIKEN RIPS. The cell has two extraction ports. The orthogonal port is for diagnostic purpose and the in-line port is for planned experiments. The extracted low-energy RI-ions are transported to an ultra-high vacuum area through the SPIG (rf six-pole ion beam guide) and bunched in the cryogenic bunching trap. The bunched ions are accelerated and mass analyzed and then delivered to different experiments. The downstream part of the inline extraction port is in its design phase at this time.

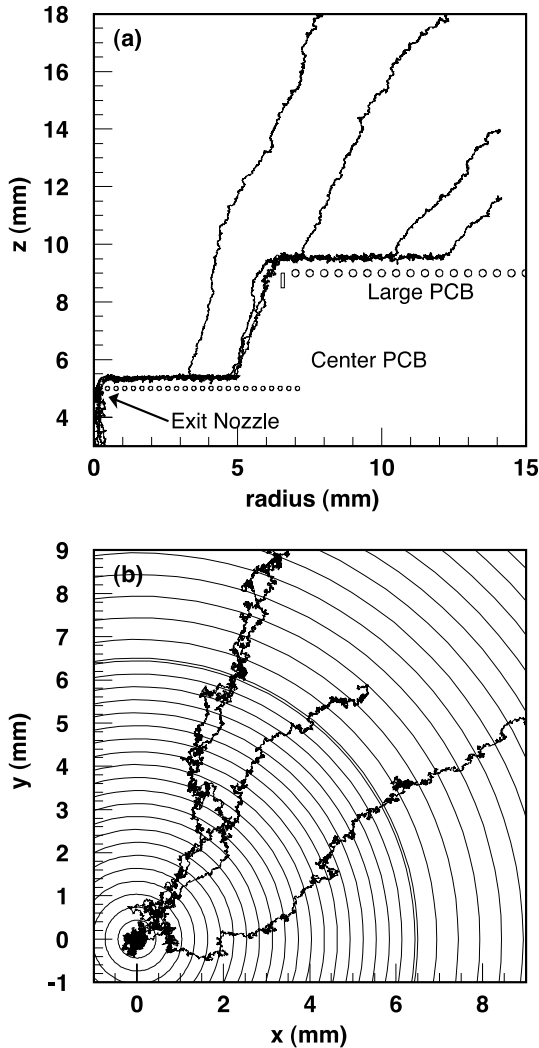


Fig. 12. Typical ion trajectories in the two layer rf-carpet as determined by microscopic particle simulation for ^8Li ions in 90 Torr He gas. The rf voltage between neighboring electrode rings is 190 V at 26 MHz. The superimposed dc field at the surface of the nozzle carpet and the upper carpet are 8 and 10 V/cm, respectively.

independently for the upper rf-carpet and for the nozzle carpet, but one of them was fixed at the optimum condition. A threshold was seen in the measurement for the nozzle similar to the off-line test (Fig. 6). The upper carpet measurement showed that the contribution from the upper carpet to the collection was only 3 times as large as that from the nozzle carpet. This predicts that

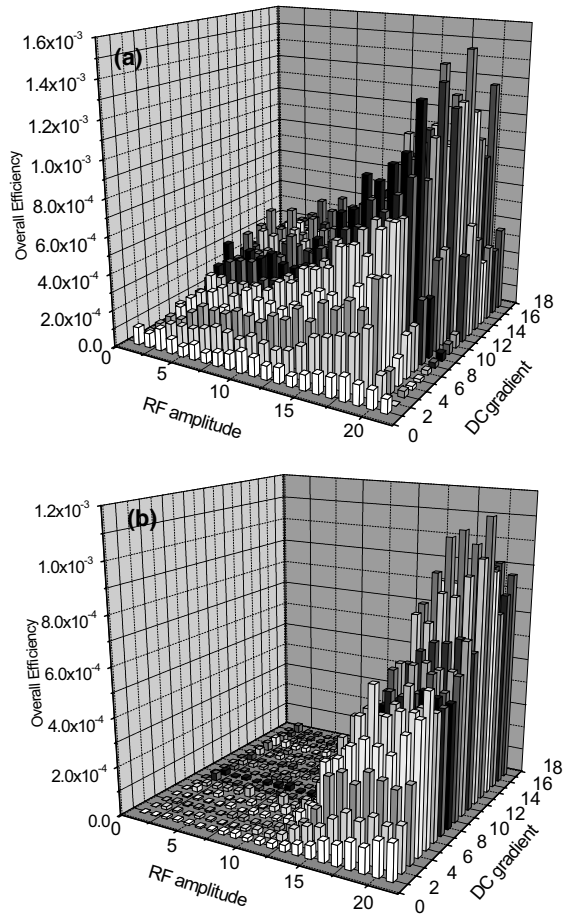


Fig. 13. Overall efficiency versus dc gradient and rf amplitude are shown: (a) for the upper large electrode with the nozzle part parameter all fixed but optimized, (b) for the nozzle electrode with the upper part parameter all fixed but optimized.

there is a problem in the transport in the upper carpet.

Fig. 14 is an experimental result for the efficiency as function of the primary beam intensity. The maximum overall efficiency of 0.2% was so far achieved when the gas pressure was 100 Torr at low beam intensity. A decrease was observed as the beam intensity was increased. This phenomena was also known in conventional IGISOL systems as a serious problem [5,18]. There are several explanations for this phenomenon [19]. A significant difference compared with IGISOL is that the decrease starts already at low intensity and the

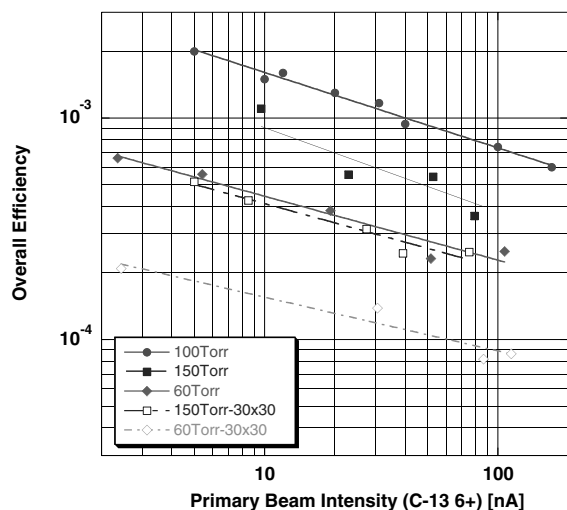


Fig. 14. The so far achieved overall efficiency for the collection of ^8Li ions as function of the primary beam intensity. The maximum efficiency of 0.2% was reached when the gas pressure was 100 Torr. The data with dashed lines correspond to measurements with a collimated beam. Such a collimated beam reduces the total energy loss but preserves the energy deposition density.

efficiency is almost inversely proportional to $I^{1/2-1/3}$ where I is the primary beam intensity. The total energy deposited when the primary beam intensity was 100 nA is estimated to be 5×10^{12} eV/s and the deposited density $\sim 10^8$ eV/s cm^3 . We also measured with a collimated beam to confirm that the effect is mainly dependent on the energy deposited density rather than the total energy loss.

5. Conclusion

We have tested the rf ion-guide system for the collection of energetic radioactive beams of the projectile fragment separator RIPS. The proof-of-principle model had a compact sized gas cell with a diameter of 10 cm and a length of 70 cm with an rf funnel structure of 10 cm aperture and a nozzle structure of 0.5 mm aperture: the model was shown to be effective for collection of ^8Li . The overall efficiency of the compact system was 10^{-4} with a gas stopping efficiency of 0.43% and a transporting efficiency of 2.4%.

A new 2 m long large cell was also tested on-line. The overall efficiency so far obtained was

0.2%. The absolute intensity of the low-energy ^8Li was more than 1000 atom per second which is sufficient for many experiments. Since the similar intensity is expected for ^{11}Be ions. We plan to start precision spectroscopy of the hyperfine structure of trapped ^{11}Be isotope aiming to study the Bohr–Weisskopf effect [20–23]. Mass measurements are also planned by using a new time-of-flight spectrometer.

Further technical development is also planned. A low-energy beam transport, a cooling trap, a mass analyzer as well as a cold-trap in the cell are under preparation. Mass analyses are essential to confirm that the dominant part of the observed radioactive ions are singly-charged atomic ions. The time profile of the extracted ions as function of the time profile of the injected beam is also important to deduce the delay time in the transportation. A cold-trap in the cell would be useful to decrease the amount of impurities in the gas. In a preliminary test with a small liquid-nitrogen trap, we have already observed an order of magnitude higher efficiency than the present performance.

Acknowledgements

We would like to thank Mr. Y. Chiba for useful suggestions concerning the rf system of the new setup and the crew of the RIKEN accelerator facility for providing the beam for the on-line test experiment. We also thank Prof. H. Wollnik for helpful discussions. The project is financially supported by Grants-in-Aid for Scientific Research from the Japan Society for the Promotion of Science.

References

- [1] Y. Yano et al., submitted.
- [2] T. Kubo, Nucl. Instr. and Meth. B, these Proceedings. doi:10.1016/S0168-583X(02)01896-7.
- [3] J. Ärje, K. Valli, Nucl. Instr. and Meth. 179 (1981) 533.
- [4] J. Ärje, J. Äystö, H. Hyvönen, P. Taskinen, V. Koponen, J. Honkanen, K. Valli, A. Hautojärvi, K. Vierinen, Nucl. Instr. and Meth. A 247 (1986) 431.
- [5] P. Dendooven, Nucl. Instr. and Meth. B 126 (1997) 182.

- [6] M. Wada, I. Katayama, Presented in the International Workshop on Ion Guide Isotope Separator On-Line (IGISOL-6), Dubna 1997, unpublished.
- [7] I. Katayama, M. Wada, H. Kawakami, J. Tanaka, K. Noda, *Hyper. Inter.* 115 (1998) 165.
- [8] M. Wada et al., in: F. Anderegge et al. (Eds.), *AIP CP606 Non-Neutral Plasma Physics IV*, 2002, p. 625.
- [9] M. Wada et al., *RIKEN Rev.* 31 (2000) 56.
- [10] H.J. Xu, M. Wada, J. Tanaka, H. Kawakami, I. Katayama, S. Ohtani, *Nucl. Instr. and Meth. A* 333 (1993) 274.
- [11] S. Fujitaka, M. Wada, H. Wang, J. Tanaka, H. Kawakami, I. Katayama, K. Ogino, H. Katsuragawa, T. Nakamura, K. Okada, S. Ohtani, *Nucl. Instr. and Meth. B* 126 (1997) 386.
- [12] S. Masuda, K. Fujibayashi, K. Ishida, in: *Advances in Static Electricity*, Auxillia SA, Brussels, 1970, p. 398.
- [13] T. Kim et al., *Anal. Chem.* 72 (2000) 2247.
- [14] E.A. Mason et al., *Phys. Rev.* 112 (1958) 445.
- [15] <http://laacg1.lanl.gov/laacg/services/possup.html>.
- [16] M. Wada, in preparation.
- [17] T. Kubo, M. Ishihara, N. Inabe, H. Kumagai, I. Tanihata, K. Yoshida, T. Nakamura, H. Okuno, S. Shimoura, K. Asahi, *Nucl. Instr. and Meth. B* 70 (1992) 309.
- [18] K. Morita, T. Inamura, T. Nomura, J. Tanaka, H. Miyatake, M. Fujioka, T. Shinozuka, M. Yoshii, H. Hama, T. Taguchi, K. Sueki, Y. Hatsukawa, K. Furuno, H. Kudo, *Nucl. Instr. and Meth. B* 26 (1987) 406.
- [19] M. Huyse, M. Facina, Y. Kudryavtsev, P. Van Duppen, ISOLDE collaboration, *Nucl. Instr. and Meth. B* 187 (2002) 535.
- [20] M. Wada, H. Xu, J. Tanaka, H. Kawakami, I. Katayama, K. Okada, S. Ohtani, *Hyperfine Interact.* 81 (1993) 161.
- [21] M. Wada, I. Katayama, H. Kawakami, J. Tanaka, S. Fujioka, Y. Ogino, H. Wang, K. Okada, T. Nakamura, S. Ohtani, *Hyperfine Interact.* 103 (1996) 59.
- [22] K. Okada, M. Wada, T. Nakamura, R. Iida, S. Ohtani, J. Tanaka, H. Kawakami, I. Katayama, *J. Phys. Soc. Jpn.* 67 (1998) 3073.
- [23] T. Nakamura, M. Wada, K. Okada, I. Katayama, S. Ohtani, H.A. Schuessler, *Opt. Commun.* 205 (2002) 329.